City Research Online

City, University of London Institutional Repository

Citation: Mullapudi, T. and Ayoub, A. (2013). Analysis of Reinforced Concrete Columns Subjected to Combined Axial, Flexure, Shear, and Torsional Loads. Journal of Structural Engineering, 139(4), pp. 561-573. doi: 10.1061/(ASCE)ST.1943-541X.0000680

This is the accepted version of the paper.

This version of the publication may differ from the final published version.

Permanent repository link: https://openaccess.city.ac.uk/id/eprint/15537/

Link to published version: http://dx.doi.org/10.1061/(ASCE)ST.1943-541X.0000680

Copyright: City Research Online aims to make research outputs of City, University of London available to a wider audience. Copyright and Moral Rights remain with the author(s) and/or copyright holders. URLs from City Research Online may be freely distributed and linked to.

Reuse: Copies of full items can be used for personal research or study, educational, or not-for-profit purposes without prior permission or charge. Provided that the authors, title and full bibliographic details are credited, a hyperlink and/or URL is given for the original metadata page and the content is not changed in any way.

City Research Online: http://openaccess.city.ac.uk/ publications@city.ac.uk

ANALYSIS OF REINFORCED CONCRETE COLUMNS SUBJECTED TO COMBINED AXIAL, FLEXURE, SHEAR AND TORSIONAL LOADS

By T R S Mullapudi[1] and Ashraf Ayoub[2]

Abstract

This paper describes the implementation of a 3-dimensional concrete constitutive model for fiber-based analysis of reinforced concrete members subjected to combined loadings including torsion. The proposed model is formulated to address the interaction between the axial force, bidirectional shear, biaxial bending, and torsion. The shear mechanism along the beam is modeled using a Timoshenko beam approach with three dimensional (3-D) frame elements with arbitrary cross-section geometry. The model considers the 3D equilibrium, compatibility, and constitutive laws of materials at the section and structural level. The concrete constitutive law follows the Softened Membrane Model (SMM) with a tangent-stiffness formulation. The emphasis of the paper is on evaluation of the effect of the different stress states on the global and local behavior of the member. The ability of the model to assess the ultimate strength, stiffness, energy dissipation, failure modes under 3-dimensional loading is evaluated by correlation of analytical results with experimental tests of RC specimens.

[1] Sr. Staff Engr., MMI Engineering Inc, Houston, TX 77077; formerly, Grad. Student, Dept. of Civ., & Envir., Engrg., Univ. of Houston, Houston, TX 77204.

[2] Assoc. Prof., Dept. of Civ., & Envir., Engrg., Univ. of Houston, Houston, TX 77204 (corresponding author).

INTRODUCTION

Reinforced concrete (RC) structures are subjected to combinations of actions and deformations, caused by spatially complex earthquake ground motions, features of structural configurations and the interaction between input and response characteristics. Combined loadings can have significant effects on the force and deformation capacity of reinforced concrete structures, resulting in unexpected large deformations and extensive damage that in turn influences the performance of structures. In particular, combined bending and torsional effect is observed in structures such as skewed and horizontally curved bridges, bridges with unequal spans or column heights, spandrel beams and bridges with outrigger beams. The analytical modeling of the behavior of structures under bending, shear and axial force interaction has received considerable attention in recent years. There is however a lack of research studies regarding the combined behavior of 3D concrete structures.

The first tests on combined shear, bending and torsion were reported by Nylander (1945). Using only longitudinal steel and disregarding transverse steel, the author found that the bending moment reduced the torsional strength. Lessig (1959) derived two possible failure modes and suggested equations for the torsional strength of the beams. Later most of the experimental work concentrated on combined loadings focused on the failure modes and the derivation of equations to define a 3-D interaction surface (Yudin 1962, Gesund and Boston 1964). Elfgren et al. (1974) derived shear, bending and torsion interaction from the Skew Bending theory; later Ewida and McMullen (1981) found that the Skew Bending theory's predictions agreed fairly well with the available results. Mansur and Paramasivam (1984) tested ten beams with small circular openings in bending and torsion and found that the torsional strength and stiffness decreased as the opening size increased. For a small amount of bending moment there is an increase in the

torsional capacity of the member but for a substantial amount of bending, the ultimate torque decreases with the increase of bending.

Rahal and Collins (1995a) studied the effect of the thickness of concrete cover on the behavior of reinforced concrete sections subjected to combined shear and torsion and found that the increase in thickness of the concrete cover increases the strength of sections, increases the crack spacing and induces lateral curvatures.

Rahal and Collins (1995b, 2003a) developed a 3-D truss model to analyze members subjected to combined loading with the help of the Modified Compression Field theory (MCFT). This model follows the curvature and checks the spalling of the concrete cover subjected to combined shear and torsional loads. Rahal and Collins (2003b) evaluated the ACI318-02 and AASHTO-LRFD provisions under combined shear and torsional loads. ACI provisions give very conservative results with the recommended 45^o angle between the compression diagonals and the longitudinal axis of the member. If a lower limit of 30^o angle is used for some cases, un-conservative results might be possible. Tirasit et al (2005) investigated the performance of ten reinforced concrete columns under cyclically applied bending and torsional loadings with and without the effect of a constant axial compression force. Axial compression increases the torsional strength and angle of cracks but its effect decreases as the rotation increases. The plastic hinge zone changes with the change of angle of twist to drift ratio; as the torsion increases, the flexural capacity and drift of the column is reduced. On the other hand, with the increase of bending moment, torsional resistance and angle of twist reduces significantly. Tirasit and Kawashima (2008) studied the effect of seismic torsion on the performance of a skewed bridge and developed the Nonlinear Torsional Hysteretic model. It was found that the torsional strength reduces the combination of flexure and eccentric impact force due to the lack of bearing

movement that induces higher torsion in bridge piers. Prakash et al. (2010) tested circular reinforced concrete columns under cyclic bending and shear, cyclic pure torsion, and various levels of combined cyclic bending, shear, and torsional loads with an aspect ratio of 3 and 6. It was found that shear capacity increases with the reduction of the aspect ratio. The displacement at ultimate shear and rotation at ultimate torque also decreased significantly under combined loading.

The establishment of nonlinear constitutive models for RC elements under combined loading and the development of corresponding nonlinear finite element models are essential to predicting the correct behavior of RC structures. In the past three decades, new constitutive models were developed in an effort to improve the general performance of the structures and elements. In these models, the equilibrium equations assume the stresses in the concrete struts and steel bars to be smeared. Similarly, the strains of steel and concrete are also smeared, and are obtained by averaging the strains along a steel bar that crosses several cracks. The constitutive laws of concrete and steel bars were developed through large-scale panel testing, and relate the smeared stresses to the smeared strains of the element (Belarbi and Hsu, 1994, 1995; Hsu and Zhang, 1996). The first work to develop such constitutive laws is the one by Vecchio and Collins (1981), who proposed the Compression Field Theory (CFT) to predict the nonlinear behavior of cracked reinforced concrete membrane elements. The CFT however is unable to take into account the tension stiffening effect of the concrete. The researchers later improved their model and developed the Modified Compression Field Theory (Vecchio and Collins 1986), in which the tension stiffening of concrete is accounted for by imposing a concrete tensile stress across the shear crack. Belarbi and Hsu (1994, 1995), and Pang and Hsu (1995) used a different approach and developed the Rotating-Angle Softened-Truss Model (RA-STM). In this model, the tension

stiffening effect of concrete was taken into account by assuming a shear stress along the crack direction. Later, the researchers improved their work and developed the Fixed-Angle Softened-Truss Model (FA-STM) (Pang and Hsu, 1996; Hsu and Zhang, 1997; and Zhang and Hsu, 1998), which is capable of predicting the concrete contribution to shear resistance by assuming the cracks to be oriented at a fixed angle. Zhu et al. (2001) derived a rational shear modulus and developed a simple solution algorithm for the FA-STM. The work was further extended by developing the Hsu/Zhu Poisson ratios (Zhu and Hsu 2002), which led to the development of the Softened Membrane Model (SMM), which can accurately predict the entire response of the specimen, including both the pre and post-peak responses. Recently, Jeng and Hsu (2009) developed the Softened Membrane Model for Torsion (SMMT) which takes into account the strain gradient of concrete struts in the shear flow zone with two significant modifications. First, in the tensile stress-stain relationship of concrete, the initial elastic modulus and strain at peak stress are increased by 45%; second, the Hsu/Zhu ratio of torsion is taken as 80% of the Hsu/Zhu ratio for bending-shear (Zhu and Hsu 2002).

Vecchio and Selby (1991) developed a finite element program for 3-D analysis of concrete structures with an eight node regular hexahedral element. In their constitutive material model they used the Modified Compression Field Theory. Gregori et al. (2007) analyzed the section of a concrete column subjected to biaxial bending, bidirectional shear and torsion by subdividing it into several regions that are subjected to either uniaxial, biaxial, or triaxial state of stress. The regions subjected to a triaxial state of stress were analyzed following the approach of Vecchio and Selby (1991).

In this research a generalized 3-D frame element adopting the Softened Membrane Model is implemented. The model is based on a Timoshenko-type force based formulation. Each element

is divided into several sections along the length and into several fibers across the cross section. Coupling between torsion and axial, flexural, and shear behavior is accounted for through satisfaction of the equilibrium and compatibility conditions along the three dimensions. This was performed by developing a new algorithm that correctly evaluates the longitudinal and transverse reinforcement strains compatible with the 3-dimensional cracked concrete behavior. The present study accomplishes three main tasks: 1) it formulates a force-based frame element to simulate the combined 3-dimensional loading effect on concrete members with reasonable computational efficiency, 2) it expands the use of the SMM constitutive model for analysis of RC members under triaxial states of stresses, 3) it validates the new finite element model by comparing its predictions with the experimental results of RC columns.

The element was added to the library of the FORTRAN based finite element analysis program FEAPpv, developed by Taylor (2005). In order to implement the 3-D model into FEAPpv, a Timoshenko beam element with triaxial constitutive relations is added to the existing library of the FEAPpv as presented in Figure1. A detailed derivation of the element formulation is presented in the next sections.

FINITE ELEMENT FORMULATION

The 3-D response is described by defining six degrees of freedom at each section of the element, which consists of three translations u_0, v_0, w_0 and three rotations $\theta_x, \theta_y, \theta_z$ with the corresponding forces N, V, W and three moments T, M_y, M_z respectively. The general 3-D beam element with rigid body modes is shown in Figure 2(a); and without rigid body modes is shown in Figure 2(b). Each element is further divided into a number of sections that are subdivided into fibers. Section deformations and forces are shown in Figure 3 (a) and Figure

3(b).

The main strains and corresponding stresses acting at any section can be grouped in vector forms:

$$\{\varepsilon\} = \{\varepsilon_x \quad \gamma_{xy} \quad \gamma_{xz}\}^T \quad \{\sigma\} = \{\sigma_x \quad \tau_{xy} \quad \tau_{xz}\}^T \tag{1}$$

where ε_x is the normal strain and γ_{xy} and γ_{xz} are the shear strains. The remaining strain vectors $\varepsilon_y, \varepsilon_z$, and γ_{yz} are determined by enforcing equilibrium between the concrete and reinforcement, as will be described later.

The section deformations at the origin of the section, in matrix form, can be written as:

$$\{s\} = \{\varepsilon_0 \quad \chi_y \quad \chi_z \quad \chi_x \quad \gamma_{xy0} \quad \gamma_{xz0}\}^T = \left\{\frac{\partial u_0}{\partial x} \quad \frac{\partial \theta_y}{\partial x} \quad -\frac{\partial \theta_z}{\partial x} \quad \frac{\partial \theta_x}{\partial x} \quad \frac{\partial v_0}{\partial x} - \theta_z \quad \frac{\partial w_0}{\partial x} + \theta_y\right\}^T \tag{2}$$

where ε_0 is the longitudinal strain at the section centroid, χ_y and χ_z are the curvatures about the y- and z- coordinate system, χ_x is the angle of twist per unit length, and γ_{xy0} and γ_{xz0} are the generalized shear strains.

The strain vector at any fiber, ε , is related to the sectional strain s as follow:

$$\{\varepsilon\} = \{\varepsilon_x \quad \gamma_{xy} \quad \gamma_{xz}\}^T = [T]\{s\} \tag{3}$$

where

$$[T] = \begin{bmatrix} 1 & z & y & 0 & 0 & 0 \\ 0 & 0 & 0 & -z & 1 & 0 \\ 0 & 0 & 0 & y & 0 & 1 \end{bmatrix}, \tag{4}$$

In the present model, a force-based formulation (Spacone et al. 1996) is adopted. The force-based approach has superior numerical capabilities than standard displacement formulations. Furthermore, the latter suffers from locking if shear deformations are accounted for. By using the

force interpolation function $\boldsymbol{b}(x)$, the section forces $\boldsymbol{s}_{(x)}$ at a section x are related to the element end forces P by:

$$\boldsymbol{S}(x) = \boldsymbol{b}(x)\boldsymbol{P} \tag{5}$$

where

$$\boldsymbol{b}(x) = \begin{bmatrix} 1 & 0 & 0 & 0 & 0 & 0 \\ 0 & 0 & \frac{x}{L}-1 & \frac{x}{L} & 0 & 0 \\ 0 & 0 & 0 & 0 & \frac{x}{L}-1 & \frac{x}{L} \\ 0 & 1 & 0 & 0 & 0 & 0 \\ 0 & 0 & 0 & 0 & \frac{-1}{L} & \frac{-1}{L} \\ 0 & 0 & \frac{-1}{L} & \frac{-1}{L} & 0 & 0 \end{bmatrix}. \tag{6}$$

To implement the force-based model in a finite element program based on displacement degrees of freedom, the following equation needs to be solved for incrementally:

$$K_{element}\Delta d = \Delta R \tag{7}$$

Here, the element stiffness matrix $K = \bar{F}^{-1}$ and the resisting load increment $\Delta R = \Delta P + F^{-1}r_u$,

Where $\bar{F} = \int_0^L b^T(x) f(x) b(x) dx$ is the element flexibility matrix, and $r_u = \int_0^L b^T(x) r_d(x) dx$ is the section residual deformation vector. The process of the state determination of force-based elements requires an internal element iteration in addition to the Newton-Raphson global iteration; it is further described by Spacone et al. (1996) and Neuenhofer and Filippou (1997).

Section behavior, as stated earlier, is evaluated through fiber discretization with the appropriate material constitutive models. The material constitutive models are described next.

CONCRETE CONSTITUTIVE MODEL

There exist six stresses $\{\sigma_{3D}\}$ and corresponding strains $\{\varepsilon_{3D}\}$ acting on any concrete fiber; however, the current formulation considers only three stresses $\{\sigma\}$ and strains $\{\varepsilon\}$ components, while the other three stress and strain components are derived by considering the equilibrium conditions. The different stress and strain vectors are defined as follow:

$$\{\sigma_{3D}\} = \{\sigma_x \quad \sigma_y \quad \sigma_z \quad \tau_{xy} \quad \tau_{yz} \quad \tau_{xz}\}^T, \ \{\varepsilon_{3D}\} = \{\varepsilon_x \quad \varepsilon_y \quad \varepsilon_z \quad \gamma_{xy} \quad \gamma_{yz} \quad \gamma_{xz}\}^T, \tag{8}$$

$$\{\sigma\} = \begin{bmatrix} \sigma_x & \tau_{xy} & \tau_{xz} \end{bmatrix}^T, \qquad \{\varepsilon\} = \begin{bmatrix} \varepsilon_x & \varepsilon_y & \gamma_{xz} \end{bmatrix}^T \tag{9}$$

$$\{\sigma_{UN}\} = \begin{bmatrix} \sigma_y & \sigma_z & \tau_{yz} \end{bmatrix}^T, \qquad \{\varepsilon_{UN}\} = \begin{bmatrix} \varepsilon_y & \varepsilon_z & \gamma_{yz} \end{bmatrix}^T \tag{10}$$

The unknown stress components σ_{UN} should equal zero to satisfy the internal equilibrium between the reinforcing steel and concrete, which will result in evaluation of the corresponding three unknown strain values ε_{UN}. Since the constrained condition is nonlinear, determination of the corresponding strains requires an iterative solution.

The proposed model extends the 2-D SMM to describe the material response of 3-D regions. The modified constitutive relations follow a 3-D stress space formulation and differ from those originally proposed in 2-D formulations (Mullapudi 2010, Mullapudi and Ayoub, 2010).

Concrete strains ε_{3D} are used to calculate the principal strains, or Eigen values; and principal strain directions, or Eigen vectors; with the help of the Jacobi method.

Eigen vectors, or direction cosines, are derived from the applied stresses σ_{3D} which are represented with $[\alpha_1]$

$$[\alpha_1] = \begin{bmatrix} l_1 & l_2 & l_3 \\ m_1 & m_2 & m_3 \\ n_1 & n_2 & n_3 \end{bmatrix} \tag{11}$$

The calculated principal strains ε_1, ε_2, ε_3 are sorted in such a way that $\varepsilon_1 > \varepsilon_2 > \varepsilon_3$, the corresponding stresses σ_1^c, σ_2^c, σ_3^c, are calculated using the biaxial constitutive relations explained in later sections.

The rotation matrix needed to rotate the stress and strain vectors from the global *x-y-z* system to the applied principal stress direction system *1-2-3* with an angle of $[\alpha_1]$ is:

$$[R(\alpha_1)] = \begin{bmatrix} l_1^2 & m_1^2 & \mathrm{n}_1^2 & l_1 m_1 & m_1 n_1 & n_1 l_1 \\ l_2^2 & m_2^2 & \mathrm{n}_2^2 & l_2 m_2 & m_2 n_2 & n_2 l_2 \\ l_3^2 & m_3^2 & \mathrm{n}_3^2 & l_3 m_3 & m_3 n_3 & n_3 l_3 \\ 2l_1 l_2 & 2m_1 m_2 & 2n_1 n_2 & l_1 m_2 + l_2 m_1 & m_1 n_2 + m_2 n_1 & n_1 l_2 + n_2 l_1 \\ 2l_2 l_3 & 2m_2 m_3 & 2n_2 n_3 & l_2 m_3 + l_3 m_2 & m_2 n_3 + m_3 n_2 & n_2 l_3 + n_3 l_2 \\ 2l_3 l_1 & 2m_3 m_1 & 2n_3 n_1 & l_3 m_1 + l_1 m_3 & m_3 n_1 + m_1 n_3 & n_3 l_1 + n_1 l_3 \end{bmatrix} \tag{12}$$

In a fiber-based element formulation, the process of the state determination at the fiber level requires the calculation of the fiber stresses $\begin{bmatrix} \sigma_x & \sigma_y & \sigma_z & \tau_{xy} & \tau_{yz} & \tau_{xz} \end{bmatrix}^T$ from the strain state $\begin{bmatrix} \varepsilon_x & \varepsilon_y & \varepsilon_z & \gamma_{xy} & \gamma_{yz} & \gamma_{xz} \end{bmatrix}^T$. Because the SMM has been implemented in a Timoshenko-type beam element, the values of ε_x, γ_{xy} and γ_{xz} are typically known, while the lateral strains ε_y and ε_z values must be evaluated from the equilibrium conditions.

EVALUATION OF LATERAL STRAIN

The equilibrium equations needed to evaluate the stresses in the *x-y-z* coordinate system $\begin{bmatrix} \sigma_x & \sigma_y & \sigma_z & \tau_{xy} & \tau_{yz} & \tau_{xz} \end{bmatrix}^T$ as a function of the principal stresses resisted by concrete

$\left[\sigma_x^c \quad \sigma_y^c \quad \sigma_z^c \quad \tau_{xy}^c \quad \tau_{yz}^c \quad \tau_{xz}^c\right]^T$ and reinforcing bar stresses f_{sx}, f_{sy} and f_{sz} along the *x*, *y*, and *z* directions respectively are:

$$\begin{aligned}\left\{\sigma_x \quad \sigma_y \quad \sigma_z \quad \tau_{xy} \quad \tau_{yz} \quad \tau_{xz}\right\}^T = \left[R(\alpha_1)\right]^{-1}\left\{\sigma_1^c \quad \sigma_2^c \quad \sigma_3^c \quad \tau_{12}^c \quad \tau_{23}^c \quad \tau_{13}^c\right\}^T \\ + \left\{\rho_{sx} f_{sx} \quad \rho_{sy} f_{sy} \quad \rho_{sz} f_{sz} \quad 0 \quad 0 \quad 0\right\}^T,\end{aligned} \tag{13}$$

where $\left\{\sigma_1^c \quad \sigma_2^c \quad \sigma_3^c \quad \tau_{12}^c \quad \tau_{23}^c \quad \tau_{13}^c\right\}^T$ is the local concrete stress vector, $\left[R\right]$ is the rotation matrix and $\left[R\right]^{-1} = \left[R\right]^T$ and ρ_{sx}, ρ_{sy} and ρ_{sz} are the smeared steel ratio in the direction of *x*, *y* and *z* respectively.

Transverse strains are internal variables determined by imposing equilibrium on each fiber between concrete and steel stirrups. Stirrup strains are not known in advance, and because of the non-linear behavior of the concrete and steel materials, an iterative procedure is needed to satisfy the equilibrium in the y and z directions, following the flow chart in Figure 4. The second of the equilibrium equations in (13) is used to evaluate the lateral strain ε_y in fiber i; taking into consideration that the value of σ_y equals zero:

$$\sigma_1^{c,i} m_1^2 + \sigma_2^{c,i} m_2^2 + \sigma_3^{c,i} m_3^2 + \tau_{12}^{c,i} 2m_1 m_2 + \tau_{23}^{c,i} 2m_2 m_3 + \tau_{31}^{c,i} 2m_1 m_3 + \rho_{sy}^i f_{sy}^i = 0 \tag{14}$$

Eq. (14) can also be written as:

$$\sigma_{cy}^i A_{cy}^i + \sigma_{sy}^i A_{sy}^i = 0 \tag{15}$$

The third of the equilibrium equations in (13) is used to evaluate the lateral strain ε_z in fiber i; taking into consideration that the value of σ_z equals zero:

$$\sigma_1^{c,i} n_1^2 + \sigma_2^{c,i} n_2^2 + \sigma_3^{c,i} n_3^2 + \tau_{12}^{c,i} 2n_1 n_2 + \tau_{23}^{c,i} 2n_2 n_3 + \tau_{31}^{c,i} 2n_3 n_1 + \rho_{sz}^i f_{sz}^i = 0 \tag{16}$$

Eq. (16) can also be written as

$$\sigma_{cz}^{i} A_{cz}^{i} + \sigma_{sz}^{i} A_{sz}^{i} = 0 \tag{17}$$

Here, σ_{cy}^{i} and σ_{cz}^{i} are the concrete stresses in the transverse y and z direction of fiber i respectively; σ_{sy}^{i} and σ_{sz}^{i} are the steel stresses in the transverse y and z direction of fiber i respectively; A_{cy}^{i} and A_{cz}^{i} are the area of concrete in y and z direction within the spacing S (Figure 5); A_{sy}^{i} and A_{sz}^{i} are the steel reinforcement, cross sectional areas in y and z direction within the spacing S ; ρ_{sy}^{i}, ρ_{sz}^{i} are the ratios of steel to concrete area in the y and z direction of fiber i , and f_{sy}^{i}, f_{sz}^{i} are the transverse steel bar stresses which are equal to σ_{sy}^{i}, and σ_{sz}^{i} .

An iterative procedure is needed to determine the lateral strain ε_y and ε_z that will also satisfy the equations demonstrated in Figure 4 because of the nonlinear behavior of the concrete and steel. An initial value for ε_y and ε_z is assumed at each fiber, and the iterations proceed until Eqs. (14 and 16) are internally satisfied.

STRAINS IN CIRCULAR SECTIONS

Circular cross sections are typically divided into a number of sectors along the circumferential direction (Figure 6).

Uni-axial stress-strain relationships of circular hoops are not available in an *x-y-z* coordinate system. Because of this difficulty they are determined along the tangential direction of the stirrup *x'-y'-z'* coordinate system and then later converted to the *x-y-z* coordinate system. In each section, the *x'-y'-z'* coordinate system is derived by choosing the angle θ' such that the *z'* axis is perpendicular to the transverse reinforcement alignment. The strain value in the *x-y-z* coordinate system is converted to the *x'-y'-z'* co-ordinate system with the help of the transformation matrix

A:

$$[A] = \begin{bmatrix} 1 & 0 & 0 \\ 0 & \cos\theta' & -\sin\theta' \\ 0 & \sin\theta' & \cos\theta' \end{bmatrix} \tag{18}$$

Accordingly, the strain perpendicular to the transverse reinforcement cross section ε_y' is calculated as:

$$\varepsilon_y' = \varepsilon_y \cos^2(\theta') - \gamma_{yz} \sin(2\theta') + \varepsilon_z \sin^2(\theta') \tag{19}$$

Having obtained the uni-axial stress and stiffness values in the *x'-y'-z'* coordinate system, these values are converted to the *x-y-z* coordinate system to satisfy equilibrium. The transverse steel reinforcement stress in the *y*-direction becomes $f_{sy} = f_y' \cos^2(\theta')$; the transverse steel reinforcement stress in the *z*-direction becomes $f_{sz} = f_y' \sin^2(\theta')$, and the shear stress contribution of the steel is neglected.

With similar transformations, the transverse steel reinforcement stiffness in the *y*-direction becomes $\bar{E}_{sy} = D_y' \cos^2(\theta')$, the transverse steel reinforcement stiffness in the *z*-direction becomes $\bar{E}_{sz} = D_y' \sin^2(\theta')$, and the shear stiffness contribution of the steel is neglected.

EVALUATION OF CONCRETE STRESS

The typical concrete stress-strain curves are derived from uni-axial tests, so the biaxial strains in the *x-y-z* direction $\begin{bmatrix} \varepsilon_x & \varepsilon_y & \varepsilon_z & \gamma_{xy} & \gamma_{yz} & \gamma_{xz} \end{bmatrix}^T$ need to be converted to equivalent uni-axial strains in the *1-2-3* direction $[\bar{\varepsilon}_1 \quad \bar{\varepsilon}_2 \quad \bar{\varepsilon}_3 \quad \gamma_{12} \quad \gamma_{23} \quad \gamma_{13}]^T$ to calculate the concrete stresses.

The biaxial principal strains are then evaluated as:

$$\{\varepsilon_1 \quad \varepsilon_2 \quad \varepsilon_3 \quad \gamma_{12} \quad \gamma_{23} \quad \gamma_{13}\}^T = [R(\alpha_1)]\{\varepsilon_x \quad \varepsilon_y \quad \varepsilon_z \quad \gamma_{xy} \quad \gamma_{yz} \quad \gamma_{xz}\}^T \tag{20}$$

Biaxial principal strains are needed to evaluate the equivalent uni-axial strains. The equivalent uni-axial strains are derived from the biaxial strains with the help of the suggested Poisson's Ratio of cracked concrete for SMM, also called the Hsu/Zhu ratios $\{\mu_{12} \quad \mu_{21} \quad \mu_{23} \quad \mu_{32} \quad \mu_{13} \quad \mu_{31}\}^T$ (Zhu and Hsu 2002). From the range of $j = 1 \text{ to } 3$ and $k = 1 \text{ to } 3$, μ_{jk} is the ratio of the resulting tensile strain increment in the principal j-direction to the source compressive strain increment in the principal k-direction; μ_{kj} is the ratio of the resulting compressive strain increment in the principal k-direction to the tensile source strain increment in the principal j-direction. The following equations were suggested by Jeng and Hsu (2009) based on comparisons of test data:

$$\mu_{jk} = 0.16 + 680\varepsilon_{sf} \qquad \varepsilon_{sf} \le \varepsilon_{yd} \tag{21}$$

$$\mu_{jk} = 1.52 \qquad \varepsilon_{sf} > \varepsilon_{yd} \tag{22}$$

$$\mu_{kj} = 0, \tag{23}$$

where ε_{sf} is defined as the strain in the reinforcement that yields first, and ε_{yd} is the yield strain of reinforcing steel.

After cracking, Hsu/Zhu ratio μ_{jk} lies outside the typical range of 0 to 0.5 for Poisson's Ratio of continuous materials; before cracking Hsu/Zhu ratio $\mu_{kj} = 0.2$, and after cracking Hsu/Zhu ratio $\mu_{kj} = 0$, indicating the tensile strain has no effect on the compressive strain.

The equivalent uni-axial strains are derived from the biaxial principal strains with Hsu/Zhu ratios $\{\mu_{12} \quad \mu_{21} \quad \mu_{23} \quad \mu_{32} \quad \mu_{13} \quad \mu_{31}\}^T$ as:

$$\{\bar{\varepsilon}_1 \quad \bar{\varepsilon}_2 \quad \bar{\varepsilon}_3\}^T = [\mu]\{\varepsilon_1 \quad \varepsilon_2 \quad \varepsilon_3\}^T, \tag{24}$$

where

$$[\mu] = \begin{bmatrix} 1 & -\mu_{12} & -\mu_{13} \\ -\mu_{21} & 1 & -\mu_{23} \\ -\mu_{31} & -\mu_{32} & 1 \end{bmatrix}^{-1} \tag{25}$$

The equivalent uni-axial strain in the longitudinal reinforcement along the x-direction with the effect of Hsu/Zhu ratio is given by:

$$\bar{\varepsilon}_{sx} = \bar{\varepsilon}_1 l_1^2 + \bar{\varepsilon}_2 l_2^2 + \bar{\varepsilon}_3 l_3^2 + \gamma_{12} 2 l_1 l_2 + \gamma_{23} 2 l_2 l_3 + \gamma_{13} 2 l_1 l_3 \tag{26}$$

The equivalent uni-axial strain in the transverse reinforcement along the y-direction with the effect of Hsu/Zhu ratio is given by:

$$\bar{\varepsilon}_{sy} = \bar{\varepsilon}_1 m_1^2 + \bar{\varepsilon}_2 m_2^2 + \bar{\varepsilon}_3 m_3^2 + \gamma_{12} 2 m_1 m_2 + \gamma_{23} 2 m_2 m_3 + \gamma_{13} 2 m_1 m_3 \tag{27}$$

The equivalent uni-axial strain in the transverse reinforcement along the z-direction with the effect of Hsu/Zhu ratio is given by:

$$\bar{\varepsilon}_{sz} = \bar{\varepsilon}_1 n_1^2 + \bar{\varepsilon}_2 n_2^2 + \bar{\varepsilon}_3 n_3^2 + \gamma_{12} 2 n_1 n_2 + \gamma_{23} 2 n_2 n_3 + \gamma_{13} 2 n_1 n_3 \tag{28}$$

The equivalent uni-axial longitudinal steel stress f_{sx}, transverse steel stresses f_{sy}, and f_{sz} are calculated from the equivalent uni-axial steel reinforcement strains $\bar{\varepsilon}_{sx}$, $\bar{\varepsilon}_{sy}$, and $\bar{\varepsilon}_{sz}$ through a smeared stress-strain relationships of mild steel bars embedded in concrete and subjected to uni-axial strains (Belarbi and Hsu 1994; 1995).

The current equivalent uni-axial strains $\bar{\varepsilon}_1$, $\bar{\varepsilon}_2$, and $\bar{\varepsilon}_3$ are individually used to calculate the concrete stresses σ_1^c, σ_2^c, and σ_3^c in the principal direction of the uni-axial concrete material stress-strain relationship.

The concrete uni-axial model describes the cyclic uni-axial constitutive relationships of cracked concrete in compression and tension and follows the modified Kent and Park model

(Park et al. 1982). The smeared stress-strain relationships of mild steel bars embedded in concrete and subjected to uni-axial strains developed by Belarbi and Hsu (1994; 1995) was used in the analysis. Steel stresses are averaged along the steel bar traversing several cracks and the resulting smeared steel stress at first yield is reduced compared to the local yield stress of a bare bar at the cracks.

CONCRETE TRIAXIAL CONSTITUTIVE RELATIONS

The constitutive equations depend on the strain state and the region of the cross section. The principal strains ε_1, ε_2, and ε_3 are found from the global strains using the Jacobi method, and the equivalent uni-axial strains $\bar{\varepsilon}_1, \bar{\varepsilon}_2$, and $\bar{\varepsilon}_3$ are derived based on the Hsu/Zhu ratio (Jeng and Hsu, 2009). The local concrete material stiffness is derived based on Young's Modulus and the Hsu/Zhu ratio. The global stiffness in Cartesian direction is calculated by transforming the local stiffness to the global direction. The global stiffness in *y*, *z*, and *yz* directions are condensed in the element formulation and, during this process, the stresses in axial, flexure, and shear directions becomes coupled.

The values of the concrete uni-axial strains in principal directions 1, 2, and 3 have eight conditions, and the strength in one direction is affected by the strain state in the other directions following the procedure proposed by Vecchio and Selby (1991). The uni-axial strains are sorted in ascending order such that $\bar{\varepsilon}_1 > \bar{\varepsilon}_2 > \bar{\varepsilon}_3$. The values of concrete compressive strength σ_1^c in direction one and concrete compressive strength σ_3^c in direction three are derived as described below, while the concrete compressive strength σ_2^c in direction two can be found in a similar way by applying the corresponding relations between the 1 and 2 directions.

For the case in which the equivalent uni-axial strain of concrete $\bar{\varepsilon}_1$ in principal direction one is in tension, and the equivalent uni-axial strain $\bar{\varepsilon}_3$ in principal direction three is in compression, the uni-axial concrete stress σ_1^c in direction one is calculated from $\bar{\varepsilon}_1$ and is not a function of the perpendicular concrete strain $\bar{\varepsilon}_3$. The compressive strength in principal direction three, however, σ_3^c will soften because of the tension in the orthogonal direction. Jeng and Hsu (2009) derived a softening equation in the tension-compression region, which is implemented in the current model, and is based on panel testing as proposed by Hsu and Zhu (2002). The equation for the compressive strength and strain reduction factor ζ is given by:

$$\zeta = \left(\frac{5.8}{\sqrt{f_c^{'}(MPa)}} \le 0.9 \right) \left(\frac{1}{\sqrt{1+400\bar{\varepsilon}_1}} \right) \left(1 - \frac{\left|\alpha_{r1}^*\right|}{32^\circ} \right) \tag{29}$$

where,
$$\alpha_{r1}^* = 0.5 \tan^{-1}\left(\frac{2\gamma_{13}}{\varepsilon_1 - \varepsilon_3} \right) \tag{30}$$

The ultimate stress in the orthogonal direction is $\zeta f_c^{'}$ at softened strain $\zeta\varepsilon_0$ when ζ is the softening coefficient; α_{r1}^* is the deviation angle in degrees; $\bar{\varepsilon}_1$ is lateral tensile strain; ε_0 is concrete strain at peak compressive strength $f_c^{'}$; and $\zeta f_c^{'}$ is the softened concrete compressive strength. If the equivalent uni-axial strain of concrete $\bar{\varepsilon}_1$ in principal direction one is in compression, and the equivalent uni-axial strain $\bar{\varepsilon}_3$ in principal direction three is in tension, the same softening equations apply to the compressive strength in direction one.

If the strains $\bar{\varepsilon}_1$ and $\bar{\varepsilon}_3$ are both in tension, σ_1^c and σ_3^c are functions only of the orthogonal concrete strains $\bar{\varepsilon}_1$ and $\bar{\varepsilon}_3$ respectively.

If the strains $\bar{\varepsilon}_1$ and $\bar{\varepsilon}_3$ are both in compression, the Vecchio's (1992) simplified version of Kupfer et al. (1969) biaxial compression strength equation is adopted, as described in details in Mullapudi and Ayoub (2010).

FIBER STATE DETERMINATION

With the equivalent uni-axial strains, the stiffness values $\bar{E}_1^c$, $\bar{E}_2^c$, and $\bar{E}_3^c$ are determined from a material uni-axial stress-strain diagram. The material constitutive equation is:

$$\left\{\sigma_{123}^c\right\} = \left[D_{lo}\right]^c \left\{\varepsilon_{123}\right\} \text{ or} \tag{31}$$

$$\left\{\sigma_1^c \quad \sigma_2^c \quad \sigma_3^c \quad \tau_{12}^c \quad \tau_{23}^c \quad \tau_{13}^c\right\}^T = \left[D_{lo}\right]^c \left\{\varepsilon_1 \quad \varepsilon_2 \quad \varepsilon_3 \quad \gamma_{12} \quad \gamma_{23} \quad \gamma_{13}\right\}^T, \tag{32}$$

Whereas $\left\{\sigma_{123}^c\right\}$ is the local concrete stress vector, $\{\varepsilon_{123}\}$ is the local principal strain vector, and $\left[D_{lo}\right]^c$ is the local uni-axial concrete material secant stiffness matrix in the principal direction, $\left[D_{pr}\right]$ is the uni-axial concrete material stiffness matrix in the normal principal directions which can be calculated as:

$$\left[D_{pr}\right] = \begin{bmatrix} 1 & -\mu_{12} & -\mu_{13} \\ -\mu_{21} & 1 & -\mu_{23} \\ -\mu_{31} & -\mu_{32} & 1 \end{bmatrix}^{-1} \begin{bmatrix} \bar{E}_1^c & 0 & 0 \\ 0 & \bar{E}_2^c & 0 \\ 0 & 0 & \bar{E}_3^c \end{bmatrix} \text{ and,} \tag{33}$$

$$\left[D_{lo}\right]^c = \begin{bmatrix} D_{pr}(1,1) & D_{pr}(1,2) & D_{pr}(1,3) & 0 & 0 & 0 \\ D_{pr}(2,1) & D_{pr}(2,2) & D_{pr}(2,3) & 0 & 0 & 0 \\ D_{pr}(3,1) & D_{pr}(3,2) & D_{pr}(3,3) & 0 & 0 & 0 \\ 0 & 0 & 0 & \dfrac{\sigma_1^c - \sigma_2^c}{\varepsilon_1 - \varepsilon_2} & 0 & 0 \\ 0 & 0 & 0 & 0 & \dfrac{\sigma_2^c - \sigma_3^c}{\varepsilon_2 - \varepsilon_3} & 0 \\ 0 & 0 & 0 & 0 & 0 & \dfrac{\sigma_1^c - \sigma_3^c}{\varepsilon_1 - \varepsilon_3} \end{bmatrix} \tag{34}$$

The concrete orthotropic stiffness matrix in the global *x*-*y*-*z* direction $\left[D_{gl}\right]^{c}$ is evaluated through the rotation matrix R :

$$\left[D_{gl}\right]^{c} = \left[R(\alpha_1)\right]^{-1}\left[D_{lo}\right]^{c}\left[R(\alpha_1)\right] \tag{35}$$

The local uni-axial reinforcement material stiffness matrix in the direction of reinforcement is given by:

$$\left[D_{gl}\right]^{sx} = \rho_{sx}\bar{E}_{sx},\ \left[D_{gl}\right]^{sy} = \rho_{sy}\bar{E}_{sy} \quad \text{and} \quad \left[D_{gl}\right]^{sz} = \rho_{sz}\bar{E}_{sz}, \tag{36}$$

where $\left[D_{gl}\right]^{sx}$ is the longitudinal steel global stiffness matrix, $\left[D_{gl}\right]^{sy}$ is the transverse steel global stiffness matrix along the *y*-axis, $\left[D_{gl}\right]^{sz}$ is the transverse steel global stiffness matrix along the *z*-axis, ρ_{sx} is the smeared area of the longitudinal steel in fiber i, ρ_{sy} is the smeared area of the transverse steel in the *y*-direction, ρ_{sz} is the smeared area of the transverse steel in the *z*-direction, and $\bar{E}_{sx}$, $\bar{E}_{sy}$, and $\bar{E}_{sz}$ are the uni-axial steel stiffnesses evaluated from the respective steel model along the longitudinal and transverse directions respectively.

The stiffness matrix including concrete and transverse steel terms is evaluated from the concrete stiffness $\left[D_{gl}\right]^{c}$, and the transverse steel stiffness $\left[D_{gl}\right]^{sy}$, $\left[D_{gl}\right]^{sz}$ as

$$\left[D_{gl}\right]^{c+sy+sz} = \left[D_{gl}\right]^{c} + \left[D_{gl}\right]^{sy} + \left[D_{gl}\right]^{sz}, \tag{37}$$

The total global stiffness matrix is non-symmetric since the off-diagonal values are affected by the Hsu/Zhu Poisson's Ratio, which depend on the stress state.

Finally, a new process for determination of the sectional and elemental stiffness matrices derived from fiber discretization is proposed in the next section.

Section and Element Stiffness and Force Evaluation

The stress and strain in the global coordinate system are as

$$\left\{\sigma_{cx} \quad \sigma_y \quad \sigma_z \quad \tau_{xy} \quad \tau_{yz} \quad \tau_{xz}\right\}^T = \left[D_{gl}\right]^{c+sy+sz} \left\{\varepsilon_x \quad \varepsilon_y \quad \varepsilon_z \quad \gamma_{xy} \quad \gamma_{yz} \quad \gamma_{xz}\right\}^T, \tag{38}$$

where the σ_{cx} is the longitudinal stress in a concrete fiber, σ_y and σ_z are the total transverse fiber stress in the y and z directions due to the concrete and steel; τ_{xy}, τ_{yz}, and τ_{xz} are the total fiber shear stresses.

The proposed fiber beam element follows the plane section hypothesis and only have x, xy, and xz degrees of freedom at the section level. The sectional degree of freedom term corresponding to the transverse strain in y-direction ε_y, transverse strain in z-direction ε_z, and shear strain γ_{yz} and corresponding stiffness and stresses are condensed out from the section stiffness matrix and load vector following the procedure described by Mullapudi and Ayoub (2010).

The fiber strains are derived from the section strains as:

$$\begin{Bmatrix} \varepsilon_x \\ \gamma_{xy} \\ \gamma_{xz} \end{Bmatrix} = \begin{bmatrix} 1 & z & y & 0 & 0 & 0 \\ 0 & 0 & 0 & -z & 1 & 0 \\ 0 & 0 & 0 & y & 0 & 1 \end{bmatrix} \left\{\varepsilon_0 \quad \chi_y \quad \chi_z \quad \chi_x \quad \gamma_{xy0} \quad \gamma_{xz0}\right\}^T \tag{39}$$

The transformation matrix to transform the fiber stiffness to the section stiffness is therefore

$$\left[T\right] = \begin{bmatrix} 1 & z & y & 0 & 0 & 0 \\ 0 & 0 & 0 & -z & 1 & 0 \\ 0 & 0 & 0 & y & 0 & 1 \end{bmatrix} \tag{40}$$

The contribution of concrete to the section stiffness is:

$$\left[(K_{Section})_c\right] = \sum \left(\left[T\right]^T \left[\bar{k}_{11}\right] \left[T\right] \right) A_{cx}, \tag{41}$$

where A_{cx} is the area of the concrete fiber in the longitudinal direction and $\bar{k}_{11}$ is the condensed

section stiffness matrix.

The sectional stiffness due to the longitudinal reinforcement is:

$$\left[(K_{Section})_{sx}\right] = \sum\left(\left[T\right]^T \left[D_{gl}\right]^{sx} \left[T\right]\right) A_{sx} \tag{42}$$

The sectional forces due to the concrete fiber are:

$$\left\{(F_{Section})_c\right\} = \sum\left(\left[T\right]^T \left\{\sigma_{fiber}\right\}_c\right) A_{cx} \tag{43}$$

The sectional forces due to the longitudinal steel fiber are:

$$\left\{\left(F_{Section}\right)_{sx}\right\} = \sum \begin{bmatrix} 1 & z & y & 0 & 0 & 0 \\ 0 & 0 & 0 & -z & 1 & 0 \\ 0 & 0 & 0 & y & 0 & 1 \end{bmatrix}^T \begin{Bmatrix} \sigma_{sx} \\ 0 \\ 0 \end{Bmatrix} A_{sx} \tag{44}$$

The total stiffness of the section is derived from the sum of concrete and steel stiffness as:

$$\left[K_{Section}\right] = \sum_1^{nc} (K_{Section})_c + \sum_1^{ns} (K_{Section})_{sx}\,, \tag{45}$$

where nc and ns are the number of concrete and longitudinal steel fibers in a section.

The total force of the section is the sum of concrete and steel forces in their respective directions:

$$\left\{F_{Section}\right\} = \sum_1^{nc} (F_{Section})_c + \sum_1^{ns} (F_{Section})_{sx} \tag{46}$$

ANALYSIS OF COLUMNS SUBJECTED TO COMBINED LOADS

The 3-D fiber beam element is used for the analysis of a combination of axial, shear, flexure, and torsion-loaded columns tested by Prakash et al. (2010). The experimental study was conducted at Missouri S&T to evaluate the behavior of reinforced concrete circular bridge columns (Figure 7) under combined flexure, axial, shear, and torsion loadings. The columns are

tested with two aspect ratios (height (H) to diameter (D)) with H/D=3 and 6, and two spiral reinforcement ratios of 0.73 percent and 1.32 percent respectively.

The actual test specimen has a diameter of 609.6 mm (24 inches) and is 3657.6 mm (144 inches) long from the top of the footing to the centerline of the applied load for the column with an aspect ratio of 6, and is 1828.8 mm (72 inches) long from the top of the footing to the centerline of the applied load for the column with an aspect ratio of 3. A 63.5 mm (2.5-inch) hole in the center of the column cross section was used to run seven high-strength steel strands that are stressed to apply an axial load of 7% of the concrete capacity (Figure 7(a)). The lateral load is applied at the top of the column using two hydraulic actuators in a displacement-control mode. The reinforcement consisted of 12 No. 8 longitudinal bars, and No. 3 spiral transverse reinforcement spaced at 69.9 mm (2.75 in.) for the columns with an aspect ratio of 6, and No. 4 spiral transverse reinforcement spaced at 69.9 mm (2.75 in.) for the columns with an aspect ratio of 3. The reinforcement details with different aspect ratios are given in Table 1.

The column section is subdivided into 36 fibers and modeled with only one element along the length. A Gauss-Labatto integration scheme with five integration points is used in the analysis. These numbers of sections and fibers proved to be sufficient to reach a converged solution. The columns boundary condition is assumed as fixed at the bottom and free at the top (Figure 7(c)). All of the columns are analyzed with a displacement-control strategy by applying a constant axial force (7% of the concrete capacity) at the top of the column with an appropriate time variant lateral displacement and twist at the top free end of the column.

The input data of the model consists of the frame geometry and boundary conditions, external loads or imposed displacements, number of sections and fibers, longitudinal and transverse reinforcement area, basic material properties (elastic modulus, yield stress and

hardening ratio for steel; compressive strength, strain at compressive strength, post-peak compression slope and tension stiffening slope for concrete), as well as time step increments. No additional data is needed.

Column H/D(6)-T/M(0.2) was tested with an applied torsion to uniaxial moment (T/M) ratio of 0.2, and an aspect ratio (H/D) of 6. The column's reinforcement ratio, concrete compressive strength and peak capacities are given in Table 2. Analysis of the column was conducted using the proposed 3D fiber beam-column element under cyclic load (Figure 8). Flexural cracks first appeared near the bottom of the column and their angle became more inclined at increasing heights above the top of the footing. The appearance of the cracks increased with an increase in applied loading. The longitudinal bars yielded at about 38 inches from the base of the column.

The model failed by yielding of the longitudinal and transverse reinforcement followed by core degradation. Figure 8 shows the comparison of the column performance with a similar column tested under pure uniaxial bending, as well as the analytical results using the proposed model. The analytical load-displacement curve matched well with the experiment. Because of the moderate amount of induced torsion, the bending strength and stiffness were reduced slightly. Figure 9 shows the longitudinal steel strain history at 432 mm (17 inches) above the foundation. The longitudinal strain increased with the increase of the lateral load acting on the column. The experimental strain gauge readings matched well with the analytical results and the model captured the yielding of the reinforcement rather well.

Another column H/D(6)-T/M(0.4) is analyzed under cyclic load with an applied torsion to moment (T/M) ratio of 0.4. The aspect ratio H/D of the column is 6. The column's reinforcement ratio, concrete compressive strength and peak capacities are given in Table 2. The column model reached the peak shear of 183.8 kN (41.3 kips) at a displacement of 196.0 mm (7.7 in) (Figure

10). For this column, both the longitudinal and transverse reinforcement yielded at same time. Because of the higher T/M ratio, damage did not only occur at the bottom of the column, but also along its entire length.

The ultimate load and peak displacement values are fairly matched with the experimental results as shown in Figure 10. There are some differences between the experimental and analytical results specifically with respect to the unloading stiffness and energy dissipation. This is due to the fact that the uniaxial concrete model of Park et al. (1982) assumes a linear unloading stiffness. The analytical results of the peak load and corresponding displacement values are compared to the experimental results in Table 3 for both, columns H/D(6)-T/M(0.2) and H/D(6)-T/M(0.4).

Column H/D(3)-T/M(0.2) with low aspect ratio H/D of 3 is analyzed with the proposed 3-D element. This column was designed to be shear sensitive, and was tested under monotonic load with an applied torsion to moment (T/M) ratio of 0.2. The column's reinforcement ratio, concrete compressive strength and peak capacities are given in Table 2. The column model reached the peak shear at a displacement of 50.8 mm (2 in) (Figure 11). The peak torsional moment in the analysis was reached at a twisting angle of 0.85 deg. (Figure 12). Before reaching the peak strength, the longitudinal steel at the bottom of the column yielded first followed by the bottom spiral reinforcement. From Figures 11 and 12, it is evident that the analytical results matched well with the experiment.

Column H/D(3)-T/M(0.4) with low aspect ratio H/D of 3 and high torsional moment characterized with T/M ratio of 0.4 was analyzed with the proposed element. The column's reinforcement ratio, concrete compressive strength and peak capacities are given in Table 2. The column model reached the peak shear at 61 mm (2.4 in) (Figure 13). The peak torsional moment

in analysis was reached at a twisting angle of 3.2 deg (Figure 14). Before reaching the peak load, the longitudinal reinforcement yielded first followed by the transverse reinforcement. Similar to the previous columns, the analytical results including the cracking, yielding, peak and ultimate loads and corresponding displacements matched well with the experimental results.

SUMMARY AND CONCLUSIONS

This work represents a finite element model for the analysis of reinforced concrete structures subjected to combined loading including torsion. A force-based Timoshenko-type 3-D beam element with SMM constitutive model was developed to analyze reinforced concrete structures with the incorporation of mechanisms of shear deformation and strength. Transverse strains due to torsion and shear were evaluated with the development of an iterative process at the fiber level, and condensed out at the section level. Circular hoop reinforcement stresses and stiffnesses were calculated based upon angular segmentation. Triaxial constitutive relations based on strain state were developed for 3-dimensional modeling of concrete fibers. The fiber state determination along with the formulation of stiffness and resisting loads were presented.

Correlation studies with available experimental test data were conducted in order to investigate the validity of the model. These studies confirmed the accuracy of the model in representing both global and local parameters as well as the proper failure mode. It was also concluded that the increase of bending moments reduces the torsional moment required to cause yielding of the transverse and longitudinal reinforcement. With the increase of the T/M ratio, the torsional stiffness degrades rapidly as compared to the flexural stiffness, and the ultimate twist is reduced. A reduction in aspect ratio reduces the displacement and twist at the ultimate resisting load, resulting in a predominantly shear failure mode.

ACKNOWLEDGEMENT

The work presented in this paper was supported by funds from the National Science Foundation under Grant number CMMI-0530737 and partially supported by the ASCE O.H. Ammann Research Fellowship. This support is gratefully acknowledged. The opinions expressed in this paper are those of the writers and do not necessarily reflect those of the sponsors.

REFERENCES

Belarbi, A. and Hsu, T.T.C., 1994, "Constitutive Laws of Concrete in Tension and Reinforcing bars Stiffened by Concrete," *ACI Structural Journal*, Vol 91, pp.465-474.

Belarbi, A. and Hsu, T.T.C., 1995, "Constitutive Laws of Softened Concrete in Biaxial Tension-Compression," *Structural Journal*, American Concrete Institute, Vol 92, No 5, pp.562-573.

Elfgren, L., Karlsson, I., and Losberg, A, 1974a, "Torsion-Bending-Shear Interaction for Concrete Beams," *Journal of the Structural Division*, ASCE, V. 100, No. ST8, pp. 1657-1676.

Ewida, A.A. and McMullen, A.E, 1982 "Concrete Members under Combined Torsion and Shear," *Journal of the Structural Division*, Vol. 108, No. 4, pp. 911-928.

Gesund, H., and Boston, L.A., 1964, "Ultimate Strength in Combined Bending and Torsion of Concrete Beams Containing Only Longitudinal Reinforcement," *Journal of Structural Division*, 61 (11), pp. 1453-1472.

Gregori, J.N., Sosa, P.M., Prada, M.A.F and Filippou, F.C., 2007 "A 3-D Numerical Model for Reinforced and Prestressed Concrete Elements Subjected to Combined Axial, Bending, Shear and Torsion Loading," *Engineering Structures*, Vol. 29, pp. 3404-3419.

Hsu, T.T.C., Zhang, L.X., 1996, "Tension Stiffening in Reinforced Concrete Membrane Elements," *Structural Journal, American Concrete Institute*, Vol 93, No 1, pp.108-115.

Hsu, T. T. C. and Zhang, L. X., 1997, "Nonlinear Analysis of Membrane Elements by Fixed-Angle Softened-Truss Model," *Structural Journal of the American Concrete Institute*, Vol. 94, No. 5, pp. 483-492.

Hsu, T. T. C. and Zhu, R. R. H., 2002, "Softened Membrane Model for Reinforced Concrete Elements in Shear," *Structural Journal of the American Concrete Institute*, Vol. 99, No. 4, pp. 460-469.

Jeng, C.H and Hsu, T.T.C., 2009, "A softened membrane model for torsion in reinforced concrete members," *Engineering Structures*, Vol. 31, No. 9, pp. 1944-54.

Kupfer, H. B., Hildorf, H. K., and Rusch, H., 1969, "Behavior of concrete under biaxial stresses," *Structural Journal, American Concrete Institute*, Vol 66, No 8, pp.656–666.

Lessig, N. N., 1959, "Determination of Load-Carrying Capacity of Rectangular Reinforced Concrete Elements Subjected to Flexure and Torsion," *Study No. 5*, Institut Betona i Zhelezobetona, Moscow, pp. 5-28.

Mansur, M.A. and Paramasivam, P., 1984, "Reinforced Concrete Beams with Small Opening in Bending and Torsion," *ACI Structural Journal*, V. 81, No. 2, Mar-April., pp. 180-185.

Mullapudi, T.R.S., Ayoub, A.S., "Modeling of the Seismic Behavior of Shear-Critical Reinforced Concrete Columns," *Journal of Engineering Structures*, 32(11), 2010, pp. 3601-15.

Mullapudi, T.R.S, 2010, "Seismic Analysis of Reinforced Concrete Structures Subjected to Combined Axial, Bending, Shear and Torsional Loads", *Ph.D. thesis*, Department of Civil and Environmental Engineering, University of Houston, Houston, 268 pp.

Neuenhofer, A., and Filippou, F.C., "Evaluation of Nonlinear Frame Finite-Element Models," *Journal of Structural Engineering*, ASCE, V. 123, No. 7, Sept.1997, pp. 958-966.

Nylander, H., 1945, "Torsion and Torsional Restraint by Concrete Structures," Bulletin D-19, *Statens Kommittee för Byggnadsforskning,* Stockholm.

Pang, X. B. and Hsu, T. T. C., 1995, "Behavior of Reinforced Concrete Membrane Elements in Shear," *Structural Journal of the American Concrete Institute,* Vol. 92, No. 6, pp. 665-679.

Pang, X. B. and Hsu, T. T. C., 1996, "Fixed-Angle Softened-Truss Model for Reinforced Concrete," *Structural Journal of the American Concrete Institute,* Vol. 93, No. 2, pp. 197-207.

Park, R, and Priestley, M.J.N, Gill, W.D., 1982, "Ductility of Square Confined Concrete Columns," *Journal of Structural Davison,* ASCE , Vol 108, No 4, pp.929-950.

Prakash, S., Belarbi, A., and You, Y., 2010, "Seismic performance of circular RC columns subjected to axial force, bending, and torsion with low and moderate shear," *Engineering Structures,* Vol. 32, pp. 46-59.

Rahal, K. N. and Collins, M. P., 1995a, "Effect of Thickness of Concrete Cover on Shear-Torsion Interaction-An Experimental Investigation," *ACI Structural Journal,* V.92, No. 3, pp. 334-342.

Rahal, K. N. and Collins, M. P., 1995b, "Analysis of Sections Subjected to Combined Shear and Torsion—A Theoretical Investigation," *ACI Structural Journal,* V. 92, No. 4, pp. 459-469.

Rahal, K. N., and Collins, M. P., 2003a, "Combined Torsion and Bending in Reinforced and Prestressed Concrete Beams," *ACI Structural Journal,* V.100, No. 2, pp. 157-165.

Rahal, K. N., and Collins, M. P., 2003b, "Experimental Evaluation of ACI and AASHTO-LRFD Design Provisions for Combined Shear and Torsion," *ACI Structural Journal,* V.100, No. 3, pp. 277-282.

Spacone, E.; Filippou, F. C.; and Taucer, F. F., 1996, "Fiber Beam-Column Model for Nonlinear Analysis of R/C Frames, Part I Formulation," *Earthquake Engineering and Structural Dynamics,* V. 25, pp. 711-725.

Taylor, R. L., 2005, "FEAP User Manual v2.0," *Department of Civil and Environmental Engineering, University of California, Berkeley, http//www.ce.berkeley.edu/~rlt/feap/*.

Tirasit, P., Kawashima, K., and Watanabe G., 2005, "An Experimental Study On The Performance Of RC Columns Subjected To Cyclic Flexural-Torsional Loading," *Proceeding of Second International Conference on Urban Earthquake Engineering, Tokyo Institute of Technology,* Tokyo, Japan, pp.357-364.

Tirasit, P., and Kawashima, K., 2008, "Effect of Nonlinear Seismic Torsion on the Performance of Skewed Bridge Piers," *Journal of Earthquake Engineering,* Vol. 12,No. 6, pp. 980-998.

Vecchio, F. J., and Collins, M. P., 1981, "Stress-Strain Characteristic of Reinforced Concrete in Pure Shear," *IABSE Colloquium, Advanced Mechanics of Reinforced Concrete, Delft,* Final Report, Zurich, Switzerland, pp. 221-225.

Vecchio, F.J., and Collins, M. P., 1986, "The Modified Compression Field Theory for Reinforced Concrete Elements Subjected to Shear," *American Concrete Institute*, Vol 83, pp.219-231.

Vecchio, F.J., Selby, R. G., 1991, "Toward Compression-Field Analysis of Reinforced Concrete Solids," *Journal of the Structural Engineering*, ASCE, V. 117, No. 6, June. , pp. 1740-1758.

Vecchio, F.J., "Finite element modeling of concrete expansion and confinement" *J. Struct. Engg, ASCE*, Vol 118, No 9, 1992, pp.2390-2405.

Yudin, V. K., 1962, "Determination of the Load-Carrying Capacity of Rectangular Reinforced Concrete Elements Subjected to Combined Torsion and Bending," *Beton i Zhelezobeton*, Moscow, No. 6, pp. 265-269.

Zhang, L.X., and Hsu, T.T.C., Jan 1998, "Behavior and Analysis of 100Mpa Concrete Membrane Elements," *J. Struct. Engg., ASCE*, V. 124, No. 1, pp. 24-34.

Zhu, R. H., Hsu, T.T.C., and Lee, J.Y., 2001, "Rational Shear Modulus for Smeared Crack Analysis of Reinforced Concrete" *Structural Journal, American Concrete Institute*, Vol 98, No 4, pp.443-450.

Zhu, R. H., and Hsu, T.T.C., 2002,"Poisson Effect of Reinforced Concrete Membrane Elements," *Structural Journal, American Concrete Institute*, Vol 99, No 5, pp.631-640.

NOTATIONS

$1-2-3$	=	direction of applied principal tensile stress
$x-y-z$	=	global coordinate of RC element
$x'-y'-z'$	=	local coordinate of RC element for circular cross section
θ'	=	angle for circular cross section
$[\ ]^T$	=	transpose matrix
$\{u_0 \quad v_0 \quad w_0 \quad \theta_x \quad \theta_y \quad \theta_z\}^T$	=	frame displacements in global system
$\{\varepsilon_x \quad \varepsilon_y \quad \varepsilon_z \quad \gamma_{xy} \quad \gamma_{yz} \quad \gamma_{xz}\}^T$	=	global strain vector
$\{\varepsilon_1 \quad \varepsilon_2 \quad \varepsilon_3 \quad \gamma_{12} \quad \gamma_{23} \quad \gamma_{13}\}^T$		biaxial principal strains in the *1-2-3* direction
$\{\sigma_x \quad \sigma_y \quad \sigma_z \quad \tau_{xy} \quad \tau_{yz} \quad \tau_{xz}\}^T$	=	global total stress vector
$\{s\} = \{\varepsilon_0 \quad \chi_y \quad \chi_z \quad \chi_x \quad \gamma_{xy0} \quad \gamma_{xz0}\}^T$	=	section deformations
$s(x) = \{N \quad V \quad W \quad T \quad M_y \quad M_z\}^T$		section forces
$\{\varepsilon\} = \{\varepsilon_x \quad \gamma_{xy} \quad \gamma_{xz}\}^T$	=	available strains

$\{\sigma\} = \{\sigma_x \quad \tau_{xy} \quad \tau_{xz}\}^T$	=	available stresses
$[T]$	=	transformation matrix
$\boldsymbol{b}(x)$	=	force interpolation function
s'	=	section deformations at $x' - y'$ coordinate system
ε_y', f_y'	=	strain and stress perpendicular to the stirrup cross section
$[A]$	=	transformation matrix for circular cross section
P	=	element end forces
d	=	element deformation
$K_{Section}(x)$	=	section stiffness matrix
$r(x)$	=	residual section deformation
r_d	=	residual of sectional deformation
r_u	=	element residual deformation vector
$f(x)$	=	section flexibility

$\bar{F}$	=	element flexibility matrix without rigid body modes
$[\alpha_1]$	=	angle between the (x-y-z) coordinate system and (1-2-3) coordinate system
$[R(\alpha_1)]$		rotating matrix
$f_{sx},\ f_{sy},\ f_{sz}$	=	Reinforcing bar stresses along the *x* , y and z directions respectively
$\rho_{sx},\ \rho_{sy},\ \rho_{sz}$	=	Smeared steel ratio in the direction of *x*, y and z directions respectively
$\{\sigma_1^c \quad \sigma_2^c \quad \sigma_3^c \quad \tau_{12}^c \quad \tau_{23}^c \quad \tau_{13}^c\}^T$	=	local concrete stress vector in $1-2-3$ direction
$\sigma_{cx}^i, \sigma_{cy}^i, \sigma_{cz}^i$	=	concrete stress in *x*, y and z directions respectively of fiber *i*
$\sigma_{sx}^i, \sigma_{sy}^i, \sigma_{sz}^i$	=	steel stress in *x*, y and z directions respectively of fiber *i*
A_{cy}^i, A_{cz}^i	=	Area of concrete between the spacing of the stirrups in the *y and z* direction respectively of fiber *i*

$A_{sy}^{i},\ A_{sz}^{i}$	=	area of steel between the spacing of the stirrups in the *y and z* direction respectively of fiber i
A_{cx}	=	area of the concrete fiber in the *x* direction.
$\{\mu_{12} \quad \mu_{21} \quad \mu_{23} \quad \mu_{32} \quad \mu_{13} \quad \mu_{31}\}^{T}$	=	Hsu/Zhu ratios
$\{\bar{\varepsilon}_1 \quad \bar{\varepsilon}_2 \quad \bar{\varepsilon}_3\}^{T}$	=	equivalent uni-axial strains
$\bar{\varepsilon}_{sx}, \bar{\varepsilon}_{sy}, \bar{\varepsilon}_{sz}$	=	equivalent uniaxial strain in the reinforcement in *x*, y and z directions respectively
ζ	=	Softened coefficient of concrete in compression
α_{r1}^{*}	=	Deviation angle between the applied stress angle α_1 and the rotating angle α_r
$f_c^{'}$	=	uni-axial concrete compressive strength
K_{c1}, K_{c2}, K_{c3}	=	biaxial strength magnification factors in *1-*, *2-*, *3-* directions respectively
$\varepsilon_{1p}, \varepsilon_{2p}, \varepsilon_{3p}$	=	ultimate strain in *1-*, *2-*, *3-* directions respectively

σ_{1p}, σ_{2p}, σ_{3p}	=	ultimate stresses in *1*-, *2*-, *3*- directions respectively
$\left[D_{pr}\right]$	=	uni-axial concrete material stiffness matrix at normal *1*-, *2*-, *3*- directions
$\left[D_{lo}\right]^{c}$	=	local uni-axial concrete material secant stiffness matrix in the principal direction
$\left[D_{gl}\right]^{c}$	=	concrete orthotropic stiffness matrix in the global *x*-*y*-*z* direction
$\left[D_{gl}\right]^{sx}$, $\left[D_{gl}\right]^{sy}$, $\left[D_{gl}\right]^{sz}$	=	steel global stiffness matrices *x*, y and z directions respectively
$\left[D_{gl}\right]^{c+sy+sz}$	=	Stiffness matrix including concrete and transverse steel terms
$\bar{E}_1^c$, $\bar{E}_2^c$, $\bar{E}_3^c$	=	concrete uni-axial stiffnesses in *1*-, *2*-, *3*- directions respectively
$\bar{E}_{sx}$, $\bar{E}_{sy}$, $\bar{E}_{sz}$	=	uni-axial steel stiffnesses along the *x*-axis, *y*-axis and z-axis respectively.
$\left[k_{fiber}\right]$	=	condensed fiber stiffness
$\left\{\sigma_{fiber}\right\}_c$	=	condensed concrete fiber stresses

$[(K_{Section})_c]$	=	Contribution of concrete to the section stiffness
$[(K_{Section})_{sx}]$	=	sectional stiffness due to the longitudinal reinforcement
$\{(F_{Section})_c\}$	=	Sectional forces due to the concrete fiber
$\{(F_{Section})_{sx}\}$	=	Sectional forces due to the longitudinal steel fiber
$[K_{Section}]$	=	total stiffness of the section
$\{F_{Section}\}$	=	total force of the section
$\{F_{Element}\}$	=	element force vector
$[K_{Element}]$	=	element stiffness matrix

Table 1. Missouri S&T Columns Reinforcement Details

Material Property	Nominal Reinforcement Size (Columns with H/D=6)			Nominal Reinforcement Size (Columns with H/D=3)	
	#3 (Spiral)	#4 (Spiral)	#8 (Longitudinal Reinforcement)	#4 (Spiral)	#8 (Longitudinal Reinforcement)
Modulus of Elasticity	226GPa (32780Ksi)	219GPa (31763Ksi)	206GPa (29878Ksi)	226GPa (32780Ksi)	206GPa (29878Ksi)
Yield Stress (0.20% Offset Method)	525 MPa(76.1Ksi)	541 MPa (78.5Ksi)	490 MPa (71.0Ksi)	525 MPa (76.1Ksi)	546 MPa (79.1Ksi)
Peak Stress	675 MPa (97.9Ksi)	693 MPa (100.5Ksi)	702 MPa (101.8Ksi)	675 MPa (97.9Ksi)	702 MPa (100.5Ksi)

Table 2. Column Details and Peak Capacities

Column Name	Spiral Reinforcement Ratio	Longitudinal Reinforcement Ratio	Concrete Compressive Strength (MPa)	Peak Shear Force (kN)	Peak Torsional Moment (kN-m)
H/D(6)-T/M(0.2)	0.73%	2.10%	41.2	214.0	155.7
H/D(6)-T/M(0.4)	0.73%	2.10%	41.2	183.8	204.0
H/D(3)-T/M(0.2)	1.32%	2.10%	28.7	448.2	159.1
H/D(3)-T/M(0.4)	1.32%	2.10%	26.8	378.0	260.8

Table 3. Load-displacement values for H/D=6, T/M =0.2 and H/D=6, T/M =0.4

	H/D=6, T/M =0.2		H/D=6, T/M =0.4	
	Displacement, mm (in)	Shear Force, KN (kip)	Displacement, mm (in)	Shear Force, KN (kip)
Analysis	221 (8.7)	214 (48.1)	196 (7.7)	183.8 (41.3)
Experiment	221.5 (8.7)	208 (46.8)	210.4 (8.3)	193.2 (43.8)

FIGURE CAPTIONS

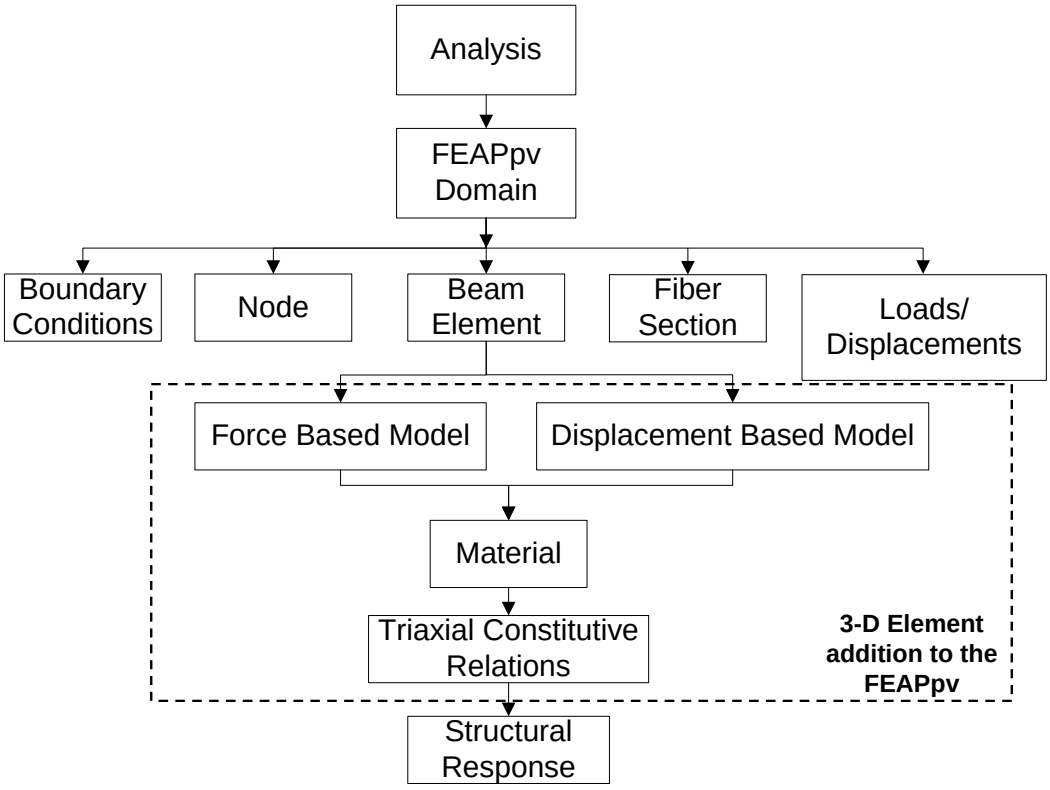

Figure 1. Implementation of 3-D Model into FEAPpv

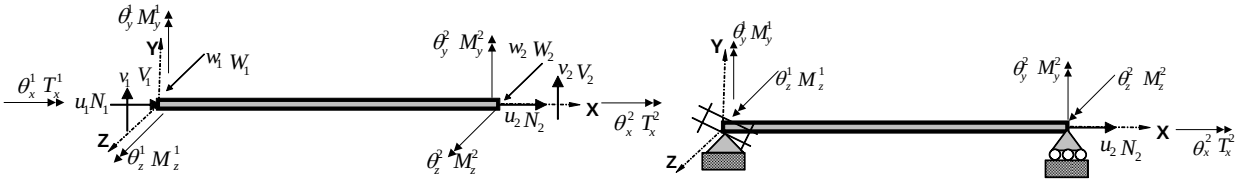

(a) (b)

Figure 2 Displacements and Forces (a) with Rigid Body Modes (b) without Rigid Body Modes

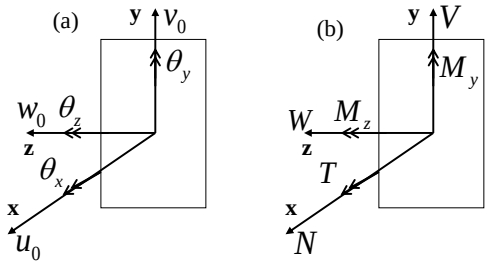

Figure 3. (a) Section Displacements (b) Section Forces

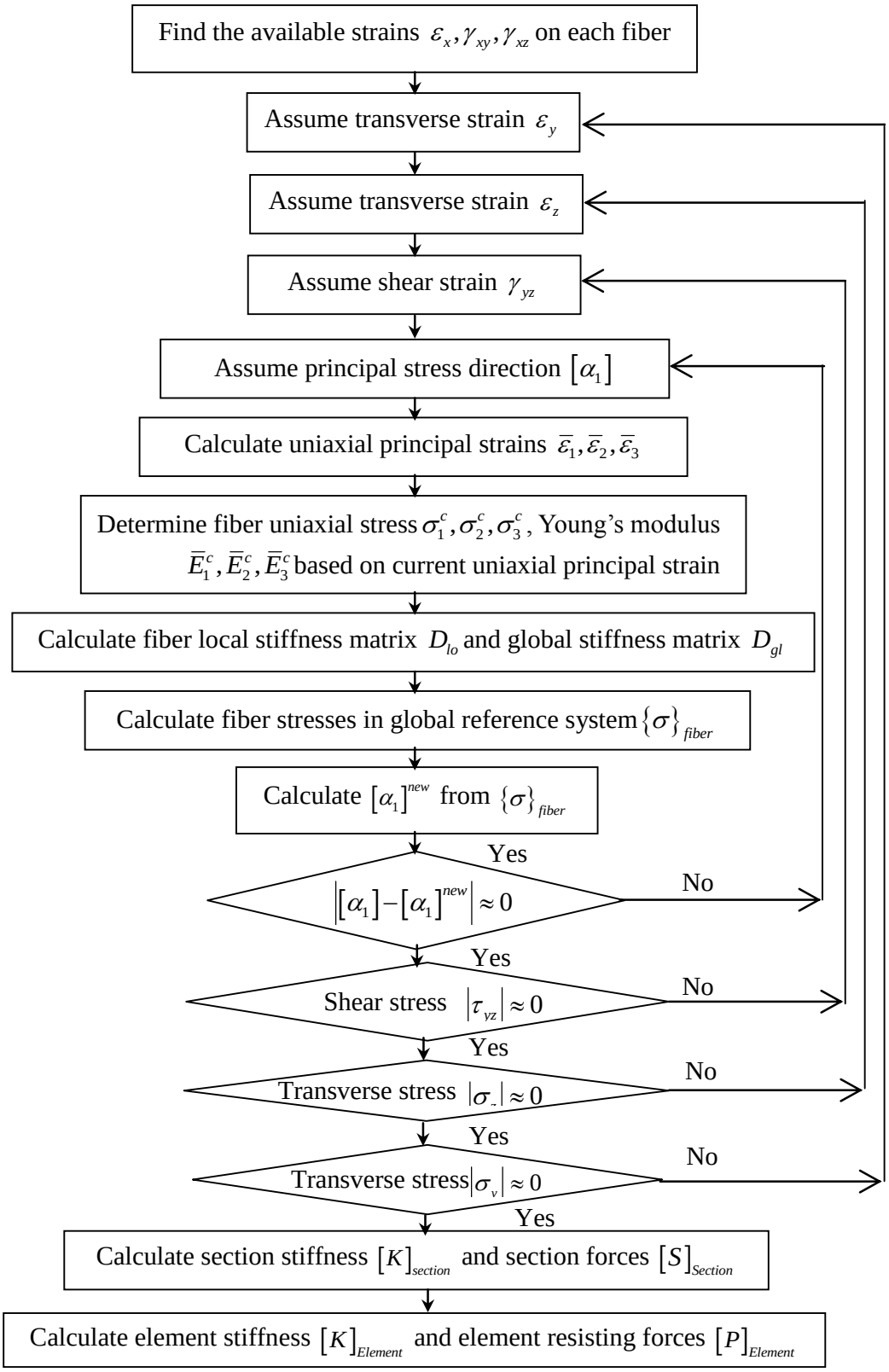

Figure 4. Iterative Procedure to Find Required 3-D Strains

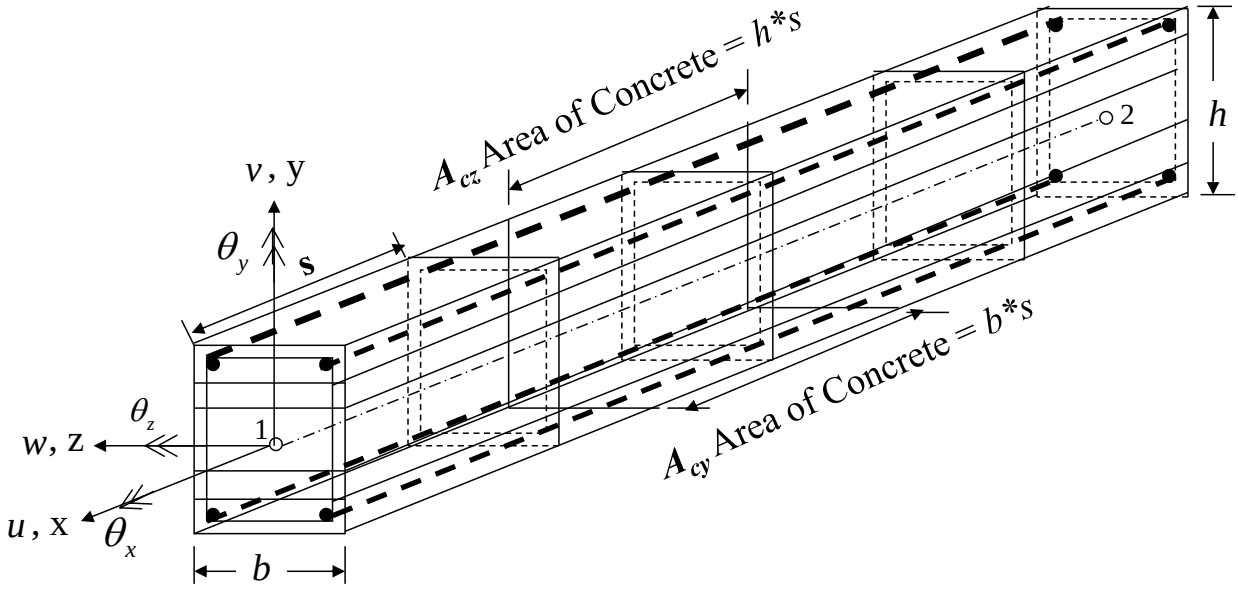

Figure 5. 3-D Fiber Element Formulation

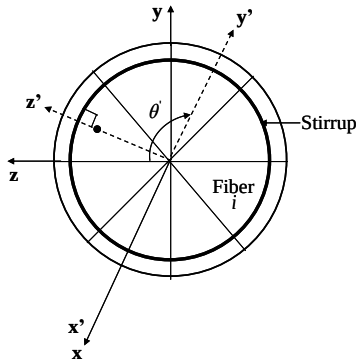

Figure 6. Circular Cross Section Transformation

(a) (b) (c)

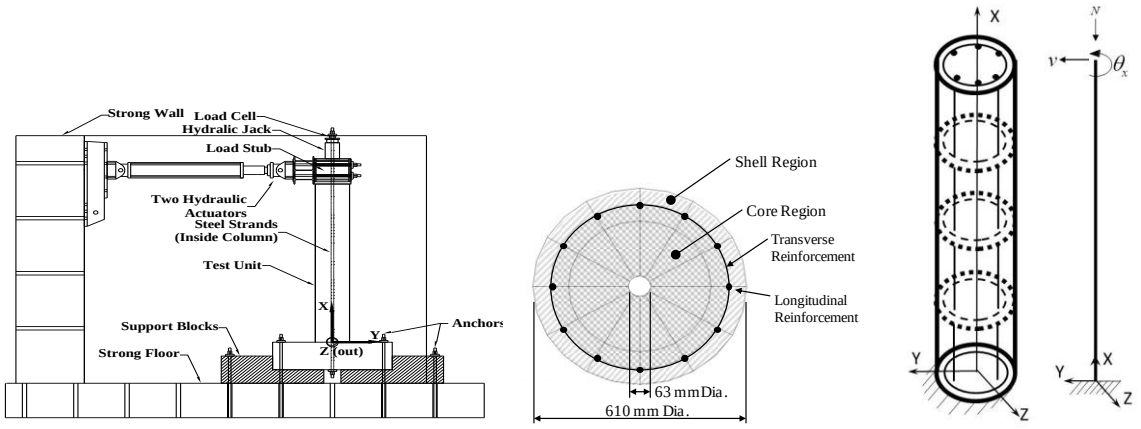

Figure 7. Bridge schematic view (a) Bridge column test setup (b) Bridge column section (c) Analysis model

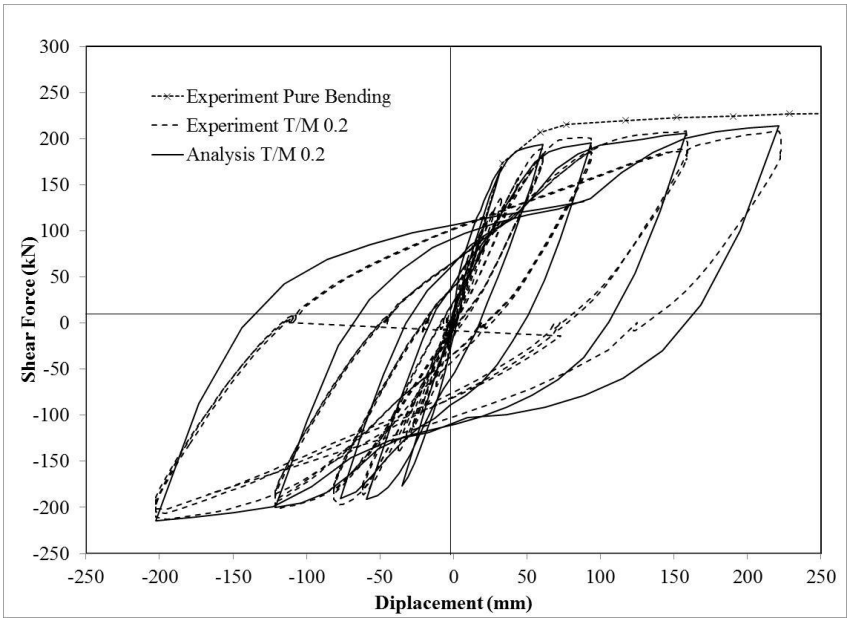

Figure 8. Cyclic load-displacement curve of column H/D(6)-T/M(0.2)

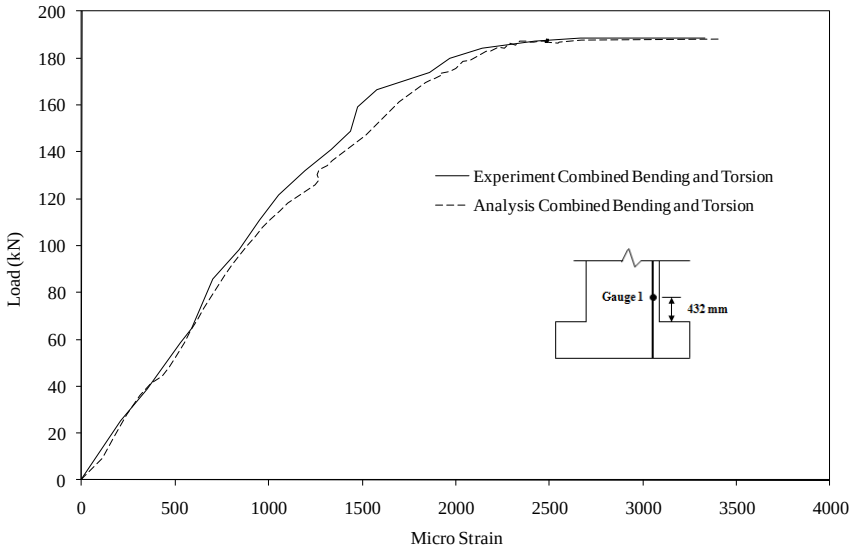

Figure 9. Longitudinal strain history at Gauge 1 location of column H/D(6)-T/M(0.2)

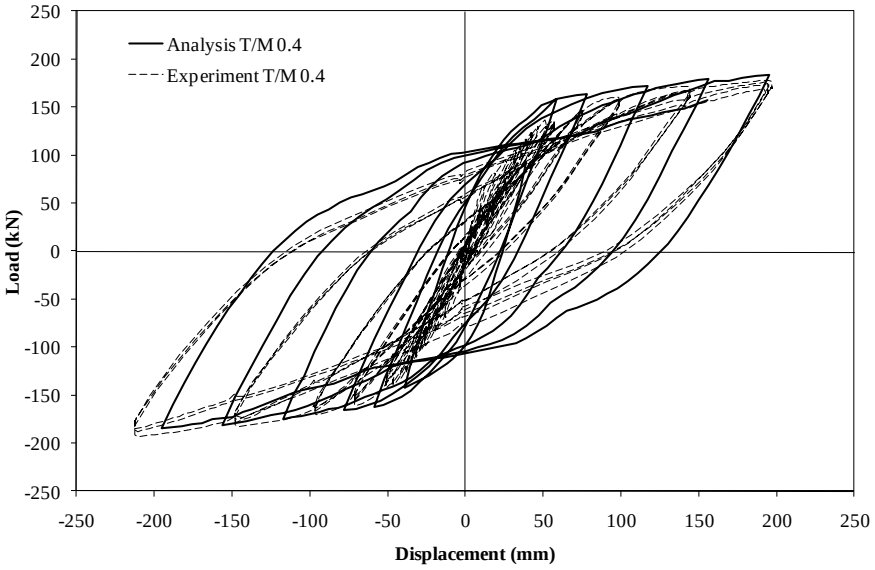

Figure 10. Cyclic load-displacement curve of column H/D(6)-T/M(0.4)

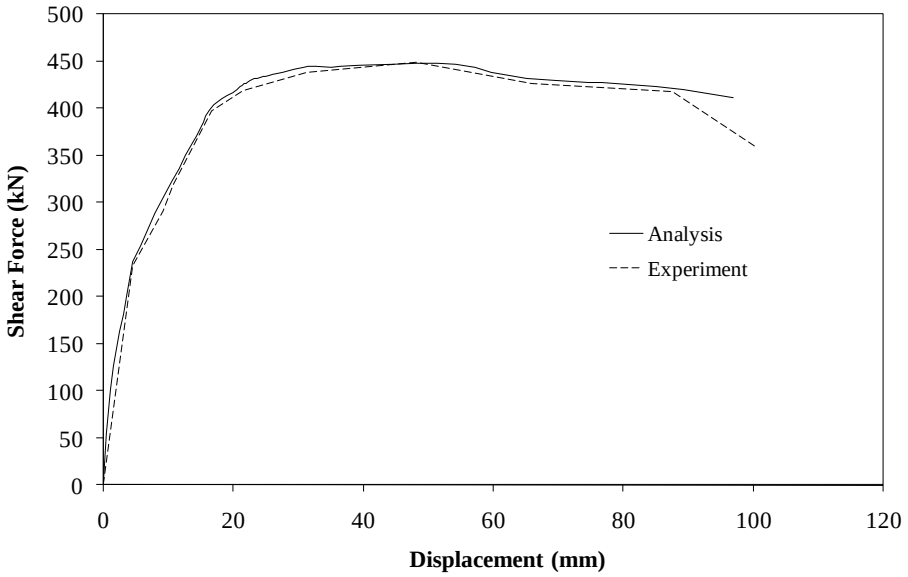

Figure 11. Monotonic load-displacement curve of column H/D(3)-T/M(0.2)

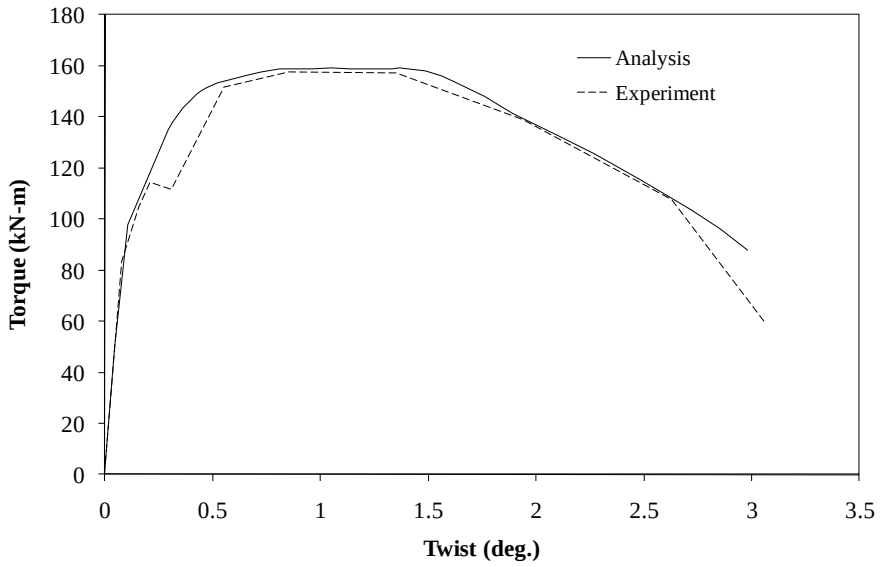

Figure 12. Monotonic torque-twist curve of column H/D(3)-T/M(0.2)

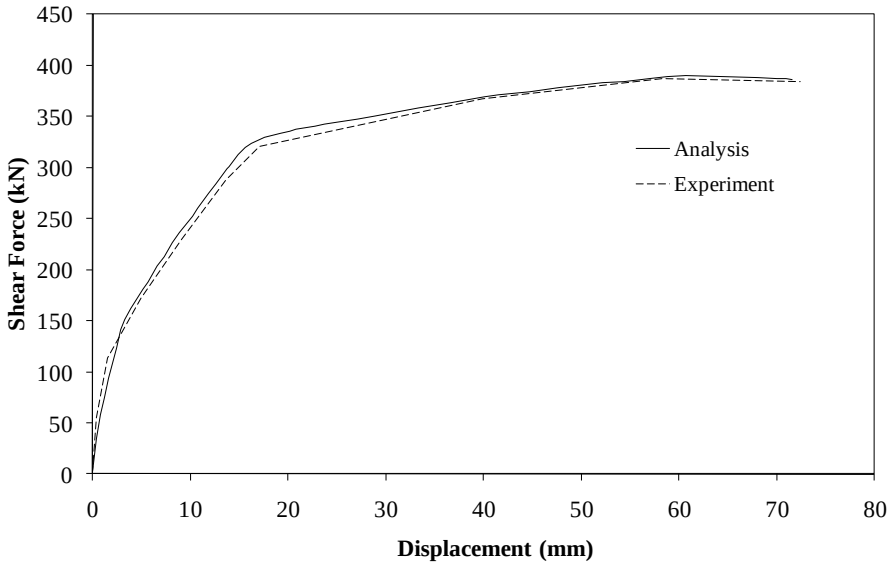

Figure 13. Monotonic load-displacement curve of column H/D(3)-T/M(0.4)

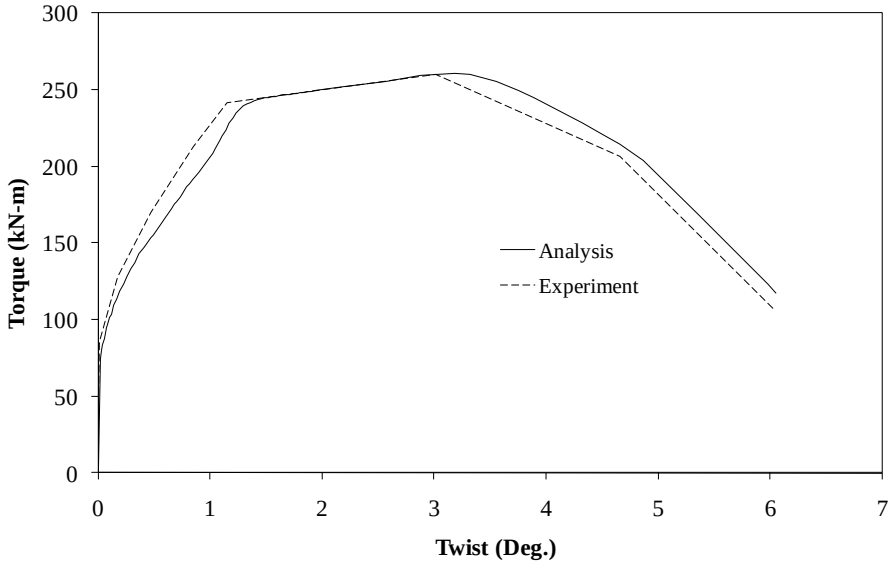

Figure 14. Monotonic torque-twist curve of column H/D(3)-T/M(0.4)